

Determination of the proton spectral function of ^{12}C from $(e, e'p)$ data

Artur M. Ankowski,¹ Omar Benhar,² and Makoto Sakuda³

¹*Institute of Theoretical Physics, University of Wrocław, 50-204 Wrocław, Poland*

²*INFN, Sezione di Roma, I-00185 Roma, Italy*

³*Physics Department, Okayama University, Okayama 700-8530, Japan*

(Dated: July 26, 2024)

The determination of the nuclear spectral function from the measured cross section of the electron-nucleus scattering process $e + A \rightarrow e' + p + (A - 1)$ is discussed, and illustrated for the case of a carbon target. The theoretical model based on the local density approximation, previously employed to derive the spectral function from a combination of accurate theoretical calculations and experimental data, has been developed further by including additional information obtained from measurements performed with high missing energy resolution. The implications for the analysis of γ -ray emission associated with nuclear deexcitation are considered.

I. INTRODUCTION

The electron-induced proton knockout reaction, in which the scattered electron and the outgoing nucleon are detected in coincidence, has long been recognised as a natural and powerful tool for the experimental determination of the spectral function describing the energy and momentum distribution of protons in the target nucleus; for a short historical account of the developments of this field of research, see Ref. [1].

Early studies of the $(e, e'p)$ cross sections provided clear cut evidence of the validity of the mean field approximation underlying the nuclear shell model, exposing at the same time its conspicuous limitations [2]. The spectroscopic lines corresponding to knockout of protons occupying the shell model orbitals were, in fact, clearly observed in the measured missing energy spectra, but the corresponding integrated strengths, providing information on the normalisation of the proton wave functions, turned out to be significantly lower than expected, regardless of the nuclear target.

In the 1970s, the spectral functions of nuclei ranging from ^{12}C to ^{58}Ni have been obtained from measurements carried out by Mougey *et al.* using the 600 MeV electron beam available at CEN Saclay [3]. These data—spanning the kinematic region corresponding to missing momentum $p_m < 320$ MeV and missing energy $E_m < 80$ MeV—have been later combined with the results of accurate nuclear matter calculations [4], to model the full p_m and E_m dependence of the spectral functions within the framework of the Local Density Approximation (LDA) [5].

The spectral function $P(\mathbf{k}, E)$ —trivially related to the two-point Green's function [6]—is an *intrinsic* property of the target nucleus, describing the probability of removing a particle of momentum \mathbf{k} from its ground state leaving the residual system with energy $E + E_0 - m$, with E_0 and m being the ground-state energy and the mass of the knocked out nucleon, respectively. As a consequence, it is a fundamental tool for the analysis of a variety of nuclear scattering processes in the kinematic region in which factorisation of the transition amplitude

is expected to be applicable. Notable applications include the electron- and neutrino-nucleus scattering cross sections; see, e.g., Refs. [5, 7–11]. It should be pointed out, however, that different reaction mechanisms and different kinematic setups are sensitive to different features of the spectral function. Theoretical analyses of inclusive (e, e') cross sections, involving integration over the phase space of the knocked out nucleon, turn out to be largely unaffected by the details of the energy dependence of $P(\mathbf{k}, E)$. On the other hand, accurate calculations of processes involving transitions between energy levels predicted by the nuclear shell model require a detailed description of the removal energy distributions, allowing to pin down the relevant spectroscopic strengths.

The authors of Ref. [10] applied the spectral function formalism in a study of γ -ray emission from deexcitation of the residual nucleus produced in $^{16}\text{O}(\nu, \nu'N)$ reactions, with N denoting either a proton or a neutron, which provides a signature of neutral-current neutrino-nucleus interactions in water-Cherenkov detectors. Their analysis employed the oxygen spectral function of Benhar *et al.* [7], obtained from the LDA-based approach of Ref. [5] using the Saclay data of Bernheim *et al.* [12]. This spectral function model allows the determination of the spectroscopic strengths of the oxygen p -states, the values of which turn out to be in remarkable agreement with those obtained from the analysis of the high-resolution missing energy spectra of the $^{16}\text{O}(e, e', p)$ process performed by Leuschner *et al.* [13].

In this article, we discuss the derivation of an improved model of the carbon spectral function of Ref. [5], designed to describe the missing energy dependence of the $^{12}\text{C}(e, e', p)$ cross section measured at NIKHEF using a 500 MeV high-duty-cycle electron beam and a pair of high-resolution spectrometers [14]. The improved spectral function model makes it possible to pin down the spectroscopic strengths of the shell model states of the carbon ground state, which are needed to extend the analysis of Ref. [10] to the case of neutral-current neutrino interactions in liquid scintillator detectors.

The remainder of this article is organised as follows. The decomposition into pole and continuum contributions and the phenomenological procedure employed to

obtain the nuclear spectral function within LDA are discussed in Sections II A and II B, respectively, whereas Section III describes the derivation of an improved model of the carbon spectral function, including the information provided by the high-resolution missing energy spectrum reported in Ref. [14]. Finally, in Section IV we summarise the results of our work and outline their applications.

II. THE NUCLEAR SPECTRAL FUNCTION

When a nucleon is knocked out from a nucleus, the residual $(A - 1)$ -particle system may be left in either a bound or a continuum state, in which at least one of the spectators is excited to a positive energy level. These two reactions mechanisms give rise to distinctively different missing energy distributions.

A. Analytic properties of the missing energy distribution

In $(e, e'p)$ processes, the missing energy is defined as

$$E_m = \omega - T_p - T_{A-1} \approx \omega - T_p, \quad (1)$$

where $\omega = E_e - E_{e'}$ denotes the electron energy loss, while T_p and T_{A-1} , with typically $T_{A-1} \ll T_p$, are the kinetic energies of the outgoing proton and the residual nucleus, respectively. Equation (1) shows that, to the extent to which Final State Interactions (FSI) between the struck nucleon and the recoiling system can be neglected or reliably described by an optical potential, the *measured* value of E_m can be identified with the removal energy of the knocked out particle. It follows that transitions to bound $(A - 1)$ -nucleon states—associated with one-particle–one-hole excitations of the target nucleus—lead to the appearance of a missing energy distribution consisting of narrow peaks corresponding to the poles of the spectral function at $E_m \approx |E_\alpha|$, with $E_\alpha < 0$ being the energy of the shell model state α . On the other hand, a smooth distribution, extending into the region of missing energies above the two-nucleon emission threshold, signals the occurrence of n -particle– n -hole excitations, with $n \geq 2$, arising from strong correlations among the nucleons in the target ground state.

Based on the above considerations, the proton spectral function can be written in *model-independent* form as

$$P(\mathbf{k}, E) = P_{\text{MF}}(\mathbf{k}, E) + P_{\text{corr}}(\mathbf{k}, E), \quad (2)$$

where P_{MF} and P_{corr} denote the pole, or mean-field (MF), and continuum, or correlation (corr), contributions, respectively. Integration over the full energy and momentum ranges yields the normalisation

$$\int d^3k dE P(\mathbf{k}, E) = Z, \quad (3)$$

with Z being the nuclear charge number.

According to the shell model, in which correlations are disregarded altogether, $P_{\text{corr}}(\mathbf{k}, E) = 0$, and the spectral function reduces to

$$P_{\text{SM}}(\mathbf{k}, E) = \sum_{\alpha \in \{F\}} |\phi_\alpha(\mathbf{k})|^2 \delta(E - |E_\alpha|). \quad (4)$$

In the above equation, $\alpha \equiv \{n_\alpha, \ell_\alpha, j_\alpha\}$ denotes the set of quantum numbers specifying the proton state α , $\phi_\alpha(\mathbf{k})$ is the corresponding unit-normalised wave function in momentum space, and the sum is extended to all states belonging to the Fermi sea $\{F\}$.

The right-hand side of Eq. (4) is substantially modified by the effects of nuclear dynamics beyond the shell model. Ground-state correlations lead to the appearance of a non-vanishing continuum contribution, which turns out to account for $\sim 20\%$ of the normalisation [4]. Furthermore, the pole contribution—the normalisation of which is obviously reduced by the same amount with respect to the shell-model prediction—is modified by the coupling between one-hole and two-hole–one-particle states of the recoiling nucleus, giving rise to a broadening of the energy distribution of the shell model states [16]. The resulting expression can be conveniently written in the form

$$P_{\text{MF}}(\mathbf{k}, E) = \sum_{\alpha \in \{F\}} |\phi_\alpha(\mathbf{k})|^2 f_\alpha(E), \quad (5)$$

with the normalisation of the finite-width distribution $f_\alpha(E)$ being given by

$$\int dE f_\alpha(E) = Z_\alpha. \quad (6)$$

The decomposition of the spectral function into discrete and continuum contributions, which follows immediately from the Källén-Léhmman representation of the two-point Green's function [15], is a powerful method for the model-independent identification of correlation effects, the size of which is gauged by the difference $[1 - (\sum_\alpha Z_\alpha)/Z] \geq 0$. A detailed discussion of this topic can be found in Ref. [16].

It should be kept in mind that, although Eqs. (2) and (5) provide a useful and physically motivated scheme for the parametrisation of the full spectral function, the width of the distributions $f_\alpha(E)$, which is known to be vanishingly small for valence states in the vicinity of the Fermi surface, becomes very large for $E_\alpha \ll E_F$, with E_F being the proton Fermi energy. As a consequence, deeply bound states turn out to be very short-lived, and their interpretation in terms of shell model orbits must be carefully analysed.

Theoretical calculations of the nuclear spectral function based on advanced microscopic models of nuclear dynamics and accurate computational techniques have been carried out for the three-nucleon system [17–19], the doubly closed shell nucleus $^{16}_8\text{O}$ [20–23], and isospin-symmetric nuclear matter [4, 24]. Calculations involving

a somewhat simplified treatment of the continuum component have been performed for ${}^4\text{He}$ [25–27]. More recently, the spectral functions of nuclei as heavy as ${}^{40}_{20}\text{Ca}$ or having significant neutron excess, such as ${}^{40}_{18}\text{Ar}$, have been also studied using the Green’s function Monte Carlo method [28].

B. Phenomenological determination of the spectral function

In the absence of FSI, the cross section of the process $e + A \rightarrow e' + p + (A - 1)$, can be written in the simple and transparent form

$$\frac{d\sigma_A}{dE_{e'}d\Omega_{e'}dE_{p'}d\Omega_{p'}} = E_{p'}|\mathbf{p}'| \sigma_{ep} P(-\mathbf{p}_m, E_m). \quad (7)$$

Here $\Omega_{e'}$ and $\Omega_{p'}$ are the solid angles specifying the directions of the scattered electron and the outgoing proton, whose energy and momentum are denoted $E_{p'}$ and \mathbf{p}' , respectively. The cross section σ_{ep} describes elastic electron scattering off a bound proton of momentum $-\mathbf{p}_m$ and removal energy E_m . The missing momentum is defined as $\mathbf{p}_m = \mathbf{q} - \mathbf{p}'$, with \mathbf{q} being the momentum transfer.

The large data set of precisely measured ($e, e'p$) cross sections collected at Saclay and NIKHEF from the 1970s to the 1980s covers mainly the kinematic region where mean-field dynamics dominates. As a consequence, Eq. (7) implies that, as long as the effects of FSI can be reliably taken into account, these data have the potential to allow an accurate determination of the spectroscopic strengths S_α , obtained from integration of the measured missing energy spectra over the regions $|E_\alpha| - \Gamma_\alpha \lesssim E_m \lesssim |E_\alpha| + \Gamma_\alpha$, with $\Gamma_\alpha > 0$ being the width of the peak of $f_\alpha(E)$ at $E \approx |E_\alpha|$. Note that, by definition, $S_\alpha \leq Z_\alpha$, because the integration of Eq. (6) is extended to all values of E . Therefore, Z_α includes contributions associated with the occurrence of two-hole–one-particle intermediate states of the residual nucleus, giving rise to the appearance of appreciable tails in the distribution $f_\alpha(E)$ [16].

In experimental analyses, the corrections originating from FSI are usually treated within the well established framework known as Distorted Wave Impulse Approximation (DWIA), based on the use of complex proton-nucleus optical potentials; for a detailed discussion of the formalism of DWIA, see, e.g., Refs. [29, 30].

Experimental studies aimed at pinning down the correlation contribution $P_{\text{corr}}(\mathbf{k}, E)$ require a careful choice of the kinematic setup, needed to minimise the background due to the occurrence of inelastic processes, as well as a more refined treatment of FSI [31]. The data collected at Jefferson Lab using a carbon target, while not providing a detailed description of the full energy and momentum dependence, show a remarkable consistency between the measured correlation strength and the missing strength in the mean-field sector observed by previous experiments [32].

The formalism based on LDA, developed by the authors of Ref. [5] in the 1990s, allows to determine the nuclear spectral function by exploiting the decomposition of Eq. (2) and the availability of accurate measurements of the mean-field contribution, Eq. (5). The main tenet underlying this approach—strongly supported by the results of both theoretical and experimental studies [33]—is that short-range nuclear dynamics, driving the appearance of correlations among the nucleons, are largely unaffected by surface and shell effects. As a consequence, correlation effects can be reliably evaluated in uniform nuclear matter.

Within LDA, the continuum component of the spectral function of a nucleus of mass number A is approximated by

$$P_{\text{corr}}^{\text{LDA}}(\mathbf{k}, E) = \int d^3r \varrho_A(\mathbf{r}) P_{\text{corr}}^{\text{NM}}[\mathbf{k}, E; \varrho = \varrho_A(\mathbf{r})], \quad (8)$$

where $\varrho_A(\mathbf{r})$ is the unit-normalised nuclear density distribution, and $P_{\text{corr}}^{\text{NM}}(\mathbf{k}, E; \varrho)$ denotes the continuum component of the spectral function of nuclear matter at density ϱ . A detailed derivation of Eq. (8) can be found in Ref. [5].

Accurate calculations of $P_{\text{corr}}^{\text{NM}}$ in the density range $0.25 \leq (\varrho/\varrho_0) \leq 1$, with $\varrho_0 \approx 0.16 \text{ fm}^{-3}$ being the equilibrium density of isospin-symmetric matter, have been carried out using an advanced many-body approach and a realistic model of the nuclear Hamiltonian [4, 5].

III. THE PROTON SPECTRAL FUNCTION OF CARBON

A. LDA model based on Saclay data

Mougey *et al.* obtained the mean-field contribution to the proton spectral function of carbon from the ($e, e'p$) data reported in Ref. [3]. Based on the combined analysis of the missing momentum and missing energy dependence of the measured cross section they were able to single out the contribution of proton knockout from different shell-model states. The peak observed at $15 \leq E_m \leq 21.5 \text{ MeV}$, associated with a maximum of the corresponding momentum distribution at $p_m \approx 100 \text{ MeV}$, was attributed to the valence p -state, whereas the strength at $30 \leq E_m \leq 50 \text{ MeV}$, whose p_m -dependence features a maximum at $p_m = 0$, was interpreted as an s -state, that is, $\ell = 0$, contribution. This decomposition allowed to extract the spectroscopic strengths of the p - and s -states from the data, corrected to take into account the effects of FSI.

The authors of Ref. [5] have combined the empirical information reported in Ref. [3] with the nuclear matter results of Ref. [4] to obtain the proton spectral function of carbon within LDA. The corresponding energy distribution, defined as

$$f_{\text{LDA}}(E) = \int d^3k [P_{\text{MF}}(\mathbf{k}, E) + P_{\text{corr}}^{\text{LDA}}(\mathbf{k}, E)], \quad (9)$$

with P_{MF} and $P_{\text{corr}}^{\text{LDA}}$ given by Eqs. (5) and (8), respectively, is displayed in Fig. 1. Note that $f(E)$ is nonzero in the region $E \geq E_{\text{thr}}$, with the proton knockout threshold E_{thr} being defined as

$$E_{\text{thr}} = |M(^{12}\text{C}) - M(^{11}\text{B}) - m_p - m_e|, \quad (10)$$

where $m_p = 938.27$ MeV and $m_e = 0.51$ MeV denote the proton and electron mass, respectively [34]. Using $M(^{12}\text{C}) = 11177.93$ MeV and $M(^{11}\text{B}) = 10255.11$ MeV [35], Eq. (10) yields $E_{\text{thr}} = 15.96$ MeV.

Integration of the distribution of Fig. 1 yields the spectroscopic factors $S_p = 2.8$ and $S_s = 1.2$, corresponding to occupation probabilities $S_\alpha/(2j_\alpha + 1) = 0.7$ and 0.6 , respectively. Note that the shell-model predicts $S_p = 4$ and $S_s = 2$.

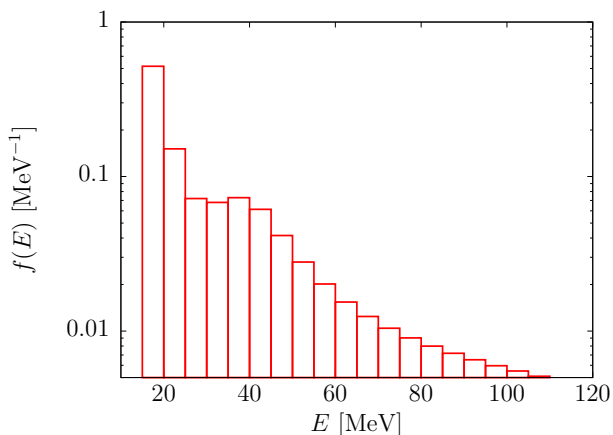


FIG. 1. Energy distribution obtained from momentum integration of the LDA spectral function of Ref. [5].

B. Parametrisation of NIKHEF data

In Ref. [14], Van der Steenhoven *et al.* reported the missing energy spectrum of the $^{12}\text{C}(e, e'p)$ reaction in the range corresponding to knock out of a proton occupying the valence p -states of carbon, measured at NIKHEF with 150 keV resolution (FWHM). The resulting distribution, $f(E_X)$, displayed in Fig. 2, exhibits three prominent peaks at excitation energy $E_X = E_m - E_{\text{thr}} = 0$ —that is, the process in which the recoiling nucleus of ^{11}B is left in its ground state—a $p_{1/2}$ state at $E_X = 2.125$ MeV, and a $p_{3/2}$ state at $E_X = 5.020$ MeV. The primary aim of this work is improving the spectral function model or Ref. [5], based on Saclay data, by inclusion of the additional information provided by the data of Ref. [14].

As a first step, the distribution of Fig. 2 has been modeled assuming gaussian-shaped peaks whose position and width, as well as the corresponding spectroscopic strengths, have been determined using a code based on the Marquardt fitting algorithm [36].

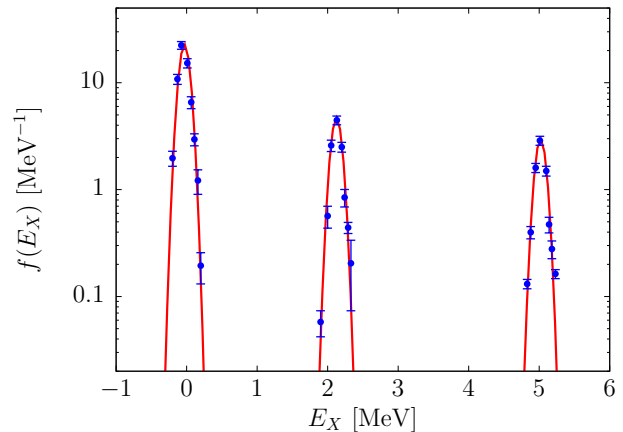


FIG. 2. Comparison between the energy distributions extracted from NIKHEF data [14] and the results of the gaussian fit employed in this work, represented by the solid lines.

In order to combine NIKHEF data with the LDA spectral function based on Saclay data, the fit shown by the solid line of Fig. 2, hereafter f_{fit} , has been renormalised in such a way as to match the p -state normalisation resulting from integration in the LDA spectral function of Ref. [5] in the range $15 \leq E_m \leq 21.5$ MeV, which will be denoted ΔE . After renormalisation, the fitted energy distribution fulfils the condition

$$\int_{\Delta E} dE_m f_{\text{fit}}(E_m) = \int_{\Delta E} dE_m f_{\text{LDA}}(E_m) = S_p, \quad (11)$$

with $S_p = 2.8$, by construction.

In Table I, the spectroscopic strengths defined as

$$S_\alpha = \int_{\Delta E_\alpha} dE_m f_{\text{fit}}(E_m), \quad (12)$$

as well as the values of the occupation probabilities of the shell-model orbits, $Z_\alpha = S_\alpha/(2j_\alpha + 1)$, are compared to the experimental results reported in Ref. [14]. Here the index α runs over the states at $E_m = 15.96$, 18.08, and 20.97 MeV, and ΔE_α is a narrow integration region designed to pin down the associated pole strength.

α	$p_{3/2}$	$p_{1/2}$	$p_{3/2}$
S_α^{expt}	1.72	0.26	0.20
Z_α^{expt}	0.43	0.13	0.05
S_α	1.747	0.273	0.201
Z_α	0.437	0.137	0.05
E_m [MeV]	15.96	18.08	20.97

TABLE I. Spectroscopic strengths and occupation probabilities of the valence p -states of ^{12}C at missing energy E_m , obtained from Eq. (12). The experimental results reported in Ref. [14] are also listed, for comparison.

The total strength, $\sum_\alpha S_\alpha = 2.22$, should be compared to value, $S_p = 2.8$ obtained from the LDA spectral function of Ref. [5]. This $\sim 25\%$ discrepancy is to be ascribed

to additional contributions arising from fragmentation of the shell-model states, clearly visible in the missing energy spectra reported in Ref. [14] and not included in the determination of the S_α from Eq. (12).

C. Improved spectral function model

The energy distribution assembled combining the fit to NIKHEF data, spanning the region $E \leq E_{\text{match}} = 21.5$ MeV, and the LDA distribution of Ref. [5] at $E > E_{\text{match}}$ is displayed by the thick solid line of Fig. 3. Comparison with the histogram representing the full distribution of Ref. [5], corresponding to Eq. (9), highlights the importance of taking into account the results of measurements performed with high missing energy resolution.

The integrated s -shell strength at $E \geq 21.5$ MeV discussed by Mougey *et al.* [3] has been also modeled, assuming a Maxwell-Boltzmann shape peaked at $E = 37$ MeV. This component, shown by the dot-dash line of Fig. 3, contributes a spectroscopic strength $S_s = 1.15$, which turns out to be within $\sim 5\%$ of the corresponding result obtained from the data of Ref. [3].

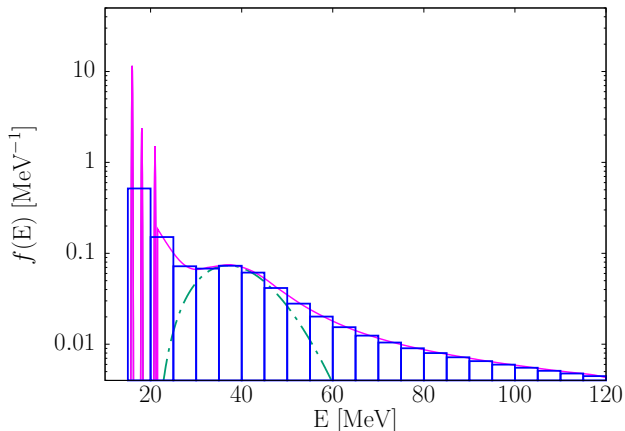


FIG. 3. The full line represents the energy distribution obtained combining the NIKHEF data at $E \leq E_{\text{match}} = 21.5$ MeV and the results of Ref. [5] at $E > E_{\text{match}}$, while the dot-dash line corresponds to the s -shell contribution described in the text. For comparison, the full distribution of Ref. [5] is shown by the histogram.

A procedure analogue to that used for deriving the energy distribution has been employed to obtain an improved model of the full spectral function. Within this scheme, $P(\mathbf{k}, E > E_{\text{match}})$ is the same as the LDA spectral function of Ref. [5], while in the region $E \leq E_{\text{match}}$ we assume the factorised form

$$P(\mathbf{k}, E < E_{\text{match}}) = n_p(\mathbf{k})f(E), \quad (13)$$

where $n_p(\mathbf{k}) = |\phi_p(\mathbf{k})|^2$ —with $\phi_p(\mathbf{k})$ being the p -state wave function in momentum space—and $f(E)$ is the distribution represented by the solid line of Fig. 3. The energy and momentum dependence of the resulting spectral

function, normalised according to Eq. (3), is illustrated in Fig. 4.

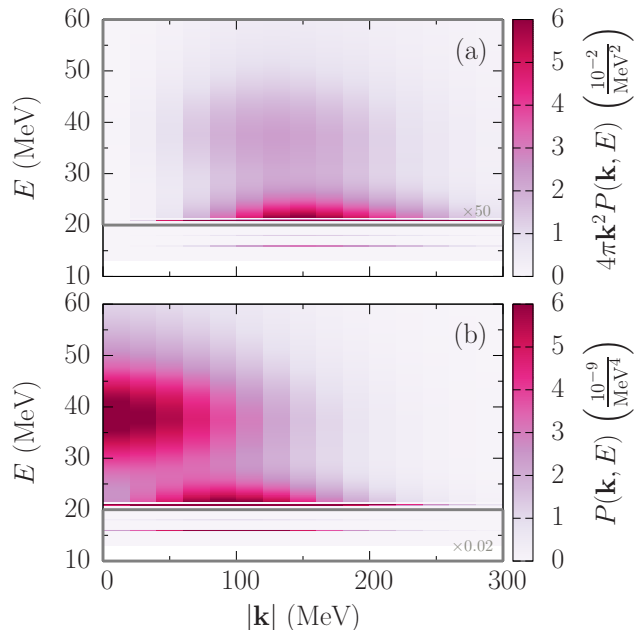


FIG. 4. Energy and momentum dependence of the carbon spectral function derived from the approach described in this work. Panels (a) and (b) have been obtained with and without including the geometric factor $4\pi\mathbf{k}^2$, respectively.

Integration of the spectral function over the energy range ΔE yields the partial momentum distribution

$$n_{\Delta E}(|\mathbf{k}|) = \int_{\Delta E} dE P(\mathbf{k}, E). \quad (14)$$

The above definition implies that suitable choices of ΔE allow to pin down the contributions of protons occupying different shell-model states, or belonging to a correlated pair in the continuum. Figure 5 shows that the partial distributions corresponding to $30 < E < 50$ MeV and $15 < E < 21.5$ MeV peak at $|\mathbf{k}| = 0$ and ~ 100 MeV, as expected for s - and p -shell protons, respectively, and become vanishingly small at momenta larger than the typical nuclear Fermi momentum $k_F \approx 250$ MeV. On the other hand, integration over the full energy range, extending up to $E = 300$ MeV, leads to the appearance of a high momentum tail originating from strong short-range correlations among the nucleons.

In Fig. 6, the p -state momentum probability obtained multiplying by a factor \mathbf{k}^2 the corresponding distribution—shown by the dashed line of Fig. 5—is compared to the experimental result reported in Ref. [3]. Note that, in order to perform a meaningful comparison, the distribution obtained from our model has been modified to account for the effects of FSI, applying the same correction employed in the analysis of Mougey *et al.* [3]. The agreement between experimental data and the results of our approach turns out to be remarkable.

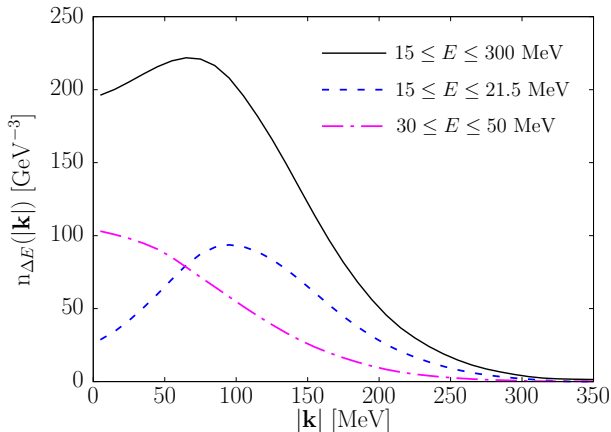


FIG. 5. Partial proton momentum distributions of carbon, obtained from Eq. (14) using the spectral function derived in this work and different integration regions ΔE . The spectroscopic factors resulting from integration of the dashed and dot-dash lines, corresponding to p - and s -shell strength, respectively, turn out to be $S_p = 2.8$ and $S_s = 1.2$.

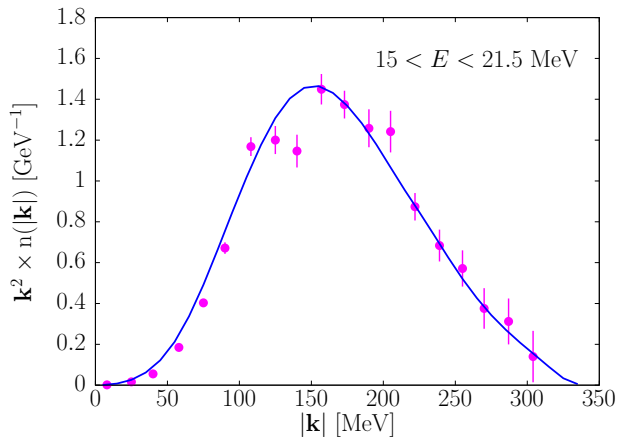


FIG. 6. Momentum probability of the p -state of ^{12}C , obtained from integration of the spectral function described in this work in the range $15 < E < 21.5$ MeV. The effects of FSI have been taken into account using the same correction applied to the data by the authors of Ref. [3].

IV. SUMMARY AND OUTLOOK

We have updated the carbon spectral function of Ref. [5]—obtained from a semi-phenomenological model based on LDA—by including additional information provided by the high-resolution $^{12}\text{C}(e, e'p)$ experiment performed at NIKHEF, Amsterdam, by Van der Steenhoven *et al.* [14].

The new spectral function features a modified energy dependence in the range at $E \leq 21.5$ MeV, relevant to removal of a p -shell proton, and reduces to the $P(\mathbf{k}, E)$ of Ref. [5] at larger E . The primary improvement lies in the capability to clearly identify the three previously unresolved states with removal energies 15.96, 18.08, and

20.97 MeV, which turn out to account for $\sim 55\%$ of the p -state strength predicted by the nuclear shell model.

The strength in the region $E > 21.5$ MeV is described in terms of an s -shell contribution—extending at energies $21.5 \lesssim E \lesssim 60$ MeV and modeled by a Maxwell-Boltzmann distribution peaked at $E \sim 37$ MeV—and a smooth background contribution, arising from fragmentation of shell-model states and nucleon-nucleon correlations, extending to energies as high as ~ 300 MeV.

It should be pointed out that the modified energy dependence of the new spectral function does not affect significantly the inclusive electron scattering cross section, the calculation of which involves integrations of $P(\mathbf{k}, E)$ over broad energy ranges.

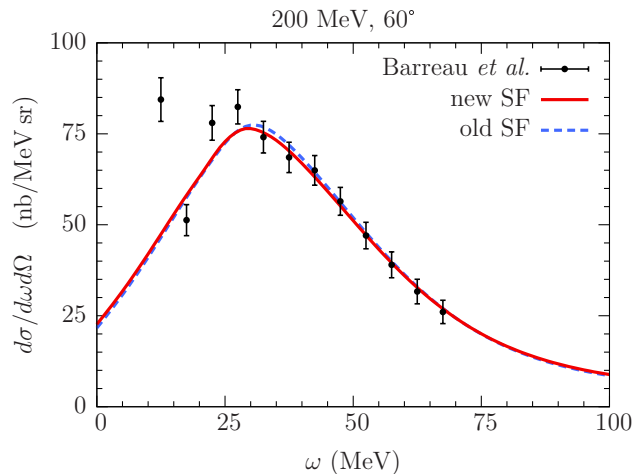


FIG. 7. Differential $^{12}\text{C}(e, e')$ cross section at beam energy $E_e = 200$ MeV and electron scattering angle $\theta_e = 60^\circ$, as a function of electron energy loss ω . Experimental data from Ref. [37].

To illustrate this point at quantitative level, we have compared the inclusive electron-carbon cross section corresponding to beam energy $E_e = 200$ MeV and electron scattering angle $\theta_e = 60^\circ$ obtained from the spectral function derived in this work to the one computed by the authors of Ref. [11] using the spectral function of Ref. [5]. It appears that the results of the two calculations are nearly indistinguishable from one another over the whole range of electron energy loss ω .

Note that the failure to reproduce the data at low ω signals the breakdown of the factorisation approximation underlying the spectral function formalism. In particular, the excitation of the giant dipole resonance at $E_X = 22.6$ MeV [38]—corresponding to $\omega = 24.2$ MeV due to nuclear recoil—is not accounted for in the calculations presented in Fig. 7. In addition, the experimental data include contributions originating from elastic scattering and transitions to discrete levels, leading to the appearance of the jump of the cross section at the lowest value of ω .

The potential of the improved $P(\mathbf{k}, E)$ can be fully exploited in studies requiring a detailed description of the

E -dependence, such as the analyses of nuclear deexcitation processes. Notable example are the calculations of the rate of γ -rays emitted by the residual nucleus in the aftermath of neutral current neutrino interactions in the quasielastic channel [10], or the identification of the leading proton kinematics in Monte Carlo cascade model simulations of FSI in neutrino-nucleus interactions [39]. The results reported in this article will allow to extend the study of Ref. [10], relevant to measurements performed using water-Cherenkov detectors, such as K2K [40], to the analysis of experiments using liquid scintillator detectors, such as KamLAND [41] and JUNO [42]. The need of accurate models of the carbon and oxygen spec-

tral functions for the description of deexcitation processes in Monte Carlo simulations has been recently discussed in Ref. [43].

ACKNOWLEDGMENTS

A.M.A. and O.B. gratefully acknowledge partial support by grant NSF PHY-1748958 to the Kavli Institute for Theoretical Physics (KITP), where this research was initiated. The work of A.M.A. is partly supported by the National Science Centre under grant UMO-2021/41/B/ST2/02778.

-
- [1] O. Benhar, “Exploring Nuclear Dynamics with $(e, e'p)$ Reactions: From LNF to JLab”, *Nuclear Physics News* **26**, 15-20 (2016). doi:10.1080/10619127.2016.1177334.
- [2] S. Frullani and J. Mougey, “Single Particle Properties of Nuclei through $(e, e'p)$ reactions”, *Adv. Nucl. Phys.* **14**, 1-283 (1984).
- [3] J. Mougey, M. Bernheim, A. Bussiere, A. Gillibert, X. H. Phan, M. Priou, D. Royer, I. Sick, and G. J. Wagner, “Quasifree $(e, e'p)$ Scattering on ^{12}C , ^{28}Si , ^{40}Ca and ^{58}Ni ”, *Nucl. Phys. A* **262**, 461-492 (1976). doi:10.1016/0375-9474(76)90510-8.
- [4] O. Benhar, A. Fabrocini and S. Fantoni, “The Nucleon Spectral Function in Nuclear Matter”, *Nucl. Phys. A* **505**, 267-299 (1989). doi:10.1016/0375-9474(89)90374-6.
- [5] O. Benhar, A. Fabrocini, S. Fantoni and I. Sick, “Spectral function of finite nuclei and scattering of GeV electrons”, *Nucl. Phys. A* **579**, 493-517 (1994). doi:10.1016/0375-9474(94)90920-2.
- [6] O. Benhar, A. Fabrocini and S. Fantoni, “Nuclear-matter Green functions in correlated-basis theory”, *Nucl. Phys. A* **550**, 201-222 (1992). doi:10.1016/0375-9474(92)90679-E.
- [7] O. Benhar, N. Farina, H. Nakamura, M. Sakuda and R. Seki, “Electron- and neutrino-nucleus scattering in the impulse approximation regime”, *Phys. Rev. D* **72**, 053005 (2005). doi:10.1103/PhysRevD.72.053005.
- [8] O. Benhar and D. Meloni, “Total neutrino and antineutrino nuclear cross sections around 1 GeV”, *Nucl. Phys. A* **789** (2007), 379-402 doi:10.1016/j.nuclphysa.2007.02.015
- [9] O. Benhar, D. Day and I. Sick, “Inclusive quasi-elastic electron-nucleus scattering”, *Rev. Mod. Phys.* **80**, 189-224 (2008). doi:10.1103/RevModPhys.80.189.
- [10] A. M. Ankowski, O. Benhar, T. Mori, R. Yamaguchi and M. Sakuda, “Analysis of γ -ray production in neutral-current neutrino-oxygen interactions at energies above 200 MeV”, *Phys. Rev. Lett.* **108**, 052505 (2012). doi:10.1103/PhysRevLett.108.052505.
- [11] A. M. Ankowski, O. Benhar and M. Sakuda, “Improving the accuracy of neutrino energy reconstruction in charged-current quasielastic scattering off nuclear targets”, *Phys. Rev. D* **91**, 033005 (2015). doi:10.1103/PhysRevD.91.033005.
- [12] M. Bernheim, A. Bussiere, J. Mougey, D. Royer, D. Tarnowski, S. Turck-Chieze, S. Frullani, S. Boffi, C. Giusti and F. D. Pacati, *et al.* “The Influence of Bound State and Optical Potentials of 1p Momentum Distributions Obtained From ^{12}C and $^{16}\text{O}(e, e'p)$ Reactions”, *Nucl. Phys. A* **375**, 381-404 (1982). doi:10.1016/0375-9474(82)90020-3.
- [13] M. Leuschner, J. R. Calarco, F. W. Hersman, E. Jans, G. J. Kramer, L. Lapikas, G. van der Steenhoven, P. K. A. de Witt Huberts, H. P. Blok and N. Kalantar-Nayestanaki, *et al.* “Quasielastic proton knockout from ^{16}O ”, *Phys. Rev. C* **49**, 955-967 (1994). doi:10.1103/PhysRevC.49.955.
- [14] G. Van der Steenhoven, H. P. Blok, E. Jans, M. De Jong, L. Lapikas, E. N. M. Quint and P. K. A. de Witt Huberts, “Knockout of 1p protons From ^{12}C Induced by the $(e, e'p)$ Reaction”, *Nucl. Phys. A* **480**, 547-572 (1988). doi:10.1016/0375-9474(88)90463-0.
- [15] A.L Fetter and J.D. Walecka, *Quantum Theory of Many-Particle Systems* (McGraw-Hill, New York, NY, 1971).
- [16] O. Benhar, A. Fabrocini and S. Fantoni, “Occupation probabilities and hole-state strengths in nuclear matter”, *Phys. Rev. C* **41**, R24-R27 (1990). doi:10.1103/PhysRevC.41.R24.
- [17] A. E. L. Dieperink, T. De Forest, I. Sick and R. A. Brandenburg, “Quasielastic electron scattering on ^3He ”, *Phys. Lett. B* **63** (1976), 261-264. doi:10.1016/0370-2693(76)90258-6.
- [18] C. Ciofi degli Atti, E. Pace and G. Salme, “Realistic nucleon-nucleon interactions and the three-body electrodisintegration of ^3He ”, *Phys. Rev. C* **21** (1980), 805-815. doi:10.1103/PhysRevC.21.805.
- [19] H. Meier-Hajduk, C. Hajduk, P. U. Sauer and W. Theis, “Quasielastic electron scattering on ^3He ”, *Nucl. Phys. A* **395** (1983), 332-348. doi:10.1016/0375-9474(83)90047-7.
- [20] W. J. W. Geurts, K. Allaart, W. H. Dickhoff and H. Muther, “Spectroscopic factors for nucleon knock-out from ^{16}O at small missing energy”, *Phys. Rev. C* **53** (1996), 2207-2212. doi:10.1103/PhysRevC.53.2207
- [21] G. A. Rijsdijk, W. J. W. Geurts, K. Allaart and W. H. Dickhoff, “Hole spectral function and two-particle-one-hole response propagator”, *Phys. Rev. C* **53** (1996), 201-213. doi:10.1103/PhysRevC.53.201.
- [22] A. Polls, M. Radici, S. Boffi, W. H. Dickhoff and H. Muther, “High momentum proton removal from ^{16}O and the $(e, e'p)$ cross section”, *Phys. Rev. C* **55** (1997), 810-819. doi:10.1103/PhysRevC.55.810.

- [23] N. Rocco and C. Barbieri, “Inclusive electron-nucleus cross section within the Self Consistent Green’s Function approach”, *Phys. Rev. C* **98** (2018) no.2, 025501 doi:10.1103/PhysRevC.98.025501.
- [24] A. Ramos, A. Polls and W. H. Dickhoff, “Single-particle properties and short-range correlations in nuclear matter”, *Nucl. Phys. A* **503** (1989), 1-52. doi:10.1016/0375-9474(89)90252-2.
- [25] C. Ciofi degli Atti and S. Liuti, “Realistic microscopic approach to deep inelastic scattering of electrons off few nucleon systems”, *Phys. Rev. C* **41** (1990), 1100-1114. doi:10.1103/PhysRevC.41.1100.
- [26] H. Morita and T. Suzuki, “A realistic spectral function of ${}^4\text{He}$ ”, *Prog. Theor. Phys.* **86** (1991), 671-684. doi:10.1143/PTP.86.671.
- [27] O. Benhar and V. R. Pandharipande, “Scattering of GeV electrons by light nuclei,” *Phys. Rev. C* **47** (1993), 2218-2227. doi:10.1103/PhysRevC.47.2218.
- [28] C. Barbieri, N. Rocco and V. Somà, “Lepton Scattering from ${}^{40}\text{Ar}$ and Ti in the quasielastic peak region,” *Phys. Rev. C* **100** (2019) no.6, 062501. doi:10.1103/PhysRevC.100.062501.
- [29] C. Giusti and F. D. Pacati, “Electron distortion in quasifree ($e, e'p$) reactions”, *Nucl. Phys. A* **473** (1987), 717-735. doi:10.1016/0375-9474(87)90276-4.
- [30] C. Giusti and F. D. Pacati, “Separation of structure functions and electron distortion in quasifree ($e, e'p$) reactions”, *Nucl. Phys. A* **485** (1988), 461-480. doi:10.1016/0375-9474(88)90548-9.
- [31] C. Barbieri, D. Rohe, I. Sick and L. Lapikas, “Effect of kinematics on final state interactions in ($e, e'p$) reactions”, *Phys. Lett. B* **608** (2005), 47-52. doi:10.1016/j.physletb.2004.12.072.
- [32] D. Rohe, C. S. Armstrong, R. Asaturyan, O. K. Baker, S. Bueltmann, C. Carasco, D. Day, R. Ent, H. C. Fenker and K. Garrow, *et al.* “Correlated strength in nuclear spectral function”, *Phys. Rev. Lett.* **93** (2004), 182501. doi:10.1103/PhysRevLett.93.182501.
- [33] M. Alvioli, C. Ciofi degli Atti and H. Morita, “Universality of nucleon-nucleon short-range correlations: the factorization property of the nuclear wave function, the relative and center-of-mass momentum distributions, and the nuclear contacts”, *Phys. Rev. C* **94** (2016), 044309. doi:10.1103/PhysRevC.94.044309.
- [34] P. A. Zyla *et al.* (Particle Data Group), “Review of Particle Physics”, *Prog. Theor. Exp. Phys.* **2020**, 083C01 (2020). doi:10.1093/ptep/ptaa104.
- [35] Nuclear Data Center, Japan Atomic Energy Agency (JAEA). <https://wwwndc.jaea.go.jp/NuC/>.
- [36] R. Bevington and D.K. Robinson, *Data reduction and error analysis for the physical sciences* (McGraw-Hill, New York, NY, 2003).
- [37] P. Barreau, M. Bernheim, J. Duclos, J. M. Finn, Z. Meziani, J. Morgenstern, J. Mougey, D. Royer, B. Saghai and D. Tarnowski, *et al.* “Deep Inelastic electron Scattering from Carbon,” *Nucl. Phys. A* **402**, 515-540 (1983). doi:10.1016/0375-9474(83)90217-8.
- [38] F. Ajzenberg-Selove, “Energy levels of light nuclei $A = 11 - 12$,” *Nuclear Physics A*, **506**, 1-158 (1990). doi:10.1016/0375-9474(90)90271-M.
- [39] A. Ershova, K. Niewczas, S. Bolognesi, A. Letourneau, J. C. David, J. L. Rodríguez-Sánchez, J. T. Sobczyk, A. Blanchet, M. B. Avanzini and J. Chakrani, *et al.* “Role of deexcitation in the final-state interactions of protons in neutrino-nucleus interactions”, *Phys. Rev. D* **108**, 112008 (2023). doi:10.1103/PhysRevD.108.112008.
- [40] J. Kameda, “Observation of deexcitation gamma rays from nuclei in 1-kton detector in K2K experiment,” *Nucl. Phys. B Proc. Suppl.* **159**, 44-49 (2006). doi:10.1016/j.nuclphysbps.2006.08.076.
- [41] S. Abe *et al.* [KamLAND], “First measurement of the strange axial coupling constant using neutral-current quasielastic interactions of atmospheric neutrinos at KamLAND,” *Phys. Rev. D* **107**, 072006 (2023). doi:10.1103/PhysRevD.107.072006.
- [42] F. An *et al.* [JUNO], “Neutrino Physics with JUNO,” *J. Phys. G* **43**, 030401 (2016). doi:10.1088/0954-3899/43/3/030401.
- [43] S. Abe, “Nuclear deexcitation simulator for neutrino interactions and nucleon decays of ${}^{12}\text{C}$ and ${}^{16}\text{O}$ based on TALYS,” *Phys. Rev. D* **109**, 036009 (2024). doi:10.1103/PhysRevD.109.036009.